Journal of Electrical Engineering, Vol. 74, No. 3, 2023, pp. 188-196

sciendo

PAPER

Pulse diffraction by a circular dielectric cylinder

Vasil Tabatadze[(a)], Oleg Drobakhin[(b)], Kamil Karaçuha[(c)]

In this article, the periodic pulse diffraction from the circular dielectric object radiated by the horn antenna is investigated and experimental verification is provided. The pulse spectrum with Hamming weight function (Hamming window) form occupies the frequency band of 38 – 52 GHz. The problem is solved using the Method of Auxiliary Sources, and the results of the computer simulation are obtained. The fundamental advantage of the method is to eliminate the singularity problem during the solution of the integral equation obtained by boundary conditions on each scatterer. The comparison is done with the experimental data, which shows good agreement between the simulation outcomes and the experimental ones. The correctness of the determination of the electric size of the object by the analysis of the scattered pulse echo serves as the verification of the approach. The outcomes reveal that less than a 3% deviation is observed between numerical and experimental analysis.

Keywords: electric size, horn antenna, MAS, object's physical properties.

1. Introduction

Determination of location and the electrical and physical properties of materials via non-invasive approaches have been studied for many years in numerous fields of engineering such as biomedical and military applications, remote sensing, security check, through-wall imaging, and standardization [1, 2]. Direct and inverse scattering problems considering electromagnetic propagation in layered media, object determination via scattering is a heavily studied concept for scientists and engineers. Specifically, two-dimensional problems in electromagnetic scattering problems interest many researchers since there exist huge numbers of topics, concepts, optimization techniques, and mathematical approaches to investigate different geometries, conditions, and cases in two-dimensional problems [1]. Since the investigation of electrical-large three-dimensional objects requires still enormous computation power, scattering by two-dimensional object play a very important role in understanding the radiation phenomena, engineering design, and applications [3, 4]. In [3, 5], fast and accurate solutions for electric and magnetic field integral equations are proposed. Especially buried objects in multilayered media and the determination of electric and physical properties of the buried material are crucial work investigated theoretically, numerically, and experimentally [6]. Besides, deep learning increases its topicality on the subject since it is very suitable for interpreting data, making sense of it, and completing missing data via deep learning [7].

To obtain the actual data via electromagnetic scattering from the region of interest, measurements should be conducted which requires interdisciplinary work. Measurements can be done via several methods such as holographic, microwave subsurface imaging, and UWB (ultrawideband) penetrating radar [8]. In [8], state-of-art approaches including artificial intelligence to determine the object's properties via electromagnetic wave propagation are presented. In [9], multi-frequency measurements are obtained to determine the dependency on a longitudinal range regarding the reflectivity analysis. Besides, the holographic approach in microwave theory was employed to obtain the size and shape of the buried object since the hologram contains the required information [10]. Apart from the investigation of the buried object in multilayered media, waveguides or resonators can be employed to determine the electric and physical properties of the materials [11]. Besides, experimentalists employ multifrequency radar with time-domain signal synthesis in their studies to collect diverse information coming from each frequency. Such an approach is very important for a buried dielectric object to catch the resonances and echoes [12, 13]. Apart from the previous studies, also Prony method is employed to determine the electrical properties of the object in the region of interest or the wall [14].

The present study investigates direct scattering by a dielectric object located in a free space using a horn antenna to determine its electrical and physical properties and is validated by experimental outcomes. The direct (or inverse) problem is solved by the method of auxiliary sources (MAS) which utilizes the shifting of the sources from the actual surface to auxiliary surfaces. This eliminates the singularity problems in the corresponding scattering integrals [15]. The methodology was first proposed by Georgian mathematician Viktor Kupradze and then, Revaz Zaridze utilized the approach in electromagnetic scattering [16, 17]. Since then,

[(a)]Informatics Institute of Istanbul Technical University, Istanbul, Türkiye
[(b)]Department of Applied Radio Physics, Electronics and Nanomaterials of Oles Honchar Dnipro National University, Dnipro, Ukraine
[(c)]Electrical Engineering Department of Istanbul Technical University, Istanbul, Türkiye
vasilitabatadze@gmail.com, drobakhino@gmail.com, karacuha17@itu.edu.tr

https://doi.org/10.2478/jee-2023-0025, Print (till 2015) ISSN 1335-3632, On-line ISSN 1339-309X

the method is not only been used for the direct problem but also, for 2D and 3D inverse problems that are solved and validated by the other methods [18, 19]. In [18], the characterization of the electrical properties of the dielectric objects is investigated by employing the method of auxiliary sources. In [19], mathematical analysis of the electromagnetic scattering field is investigated and the approaches are promising in employing the determination of the electrical properties of the objects. In this article, the method of auxiliary sources is validated by the experimental outcomes. In the numerical analysis part, the novelty is that the horn antenna is included together with the cylinder source.

In previous works in MAS, pure sources such as a plane or cylindrical waves are employed as the incident fields [18]. However, in this paper, a pulse source is used for the excitation and is located inside the horn antenna which gives better agreement with experiments. The advantage of the proposed method is being more efficient in the sense of the computational complexity than the well-known method the method of moments (MoM) [20, 21] since the sources are shifted from the real physical surface and the singularity problems in the integral equations obtained by the boundary condition are eliminated. In the present study, Hamming weight function is employed as the form of a spectrum of the incident signal from the horn antenna in a limited frequency band of 38-52 GHz. Then, echoes of the scattered field are measured and from the echo amplitude, width, and location, the electrical size and/or properties of the object can be determined or predicted.

The study follows the formulation of the problem section in which the geometry of the problem and mathematical background is provided. Then, details regarding the experiment are given. Later, numerical results and a comparison between the numerical and experimental results are provided. Finally, the conclusion is drawn.

2. Formulation of the problem

The study investigates electromagnetic scattering by dielectric objects. A horn antenna is utilized for the source of electromagnetic waves and measurement from the scattered field is also obtained from the horn antenna. Therefore, the theoretical part is also developed for such scenarios. The main aim of this part is to be able to express the incident and scattered electric field in a mathematical form. First, the incident electric field would be explained. Its frequency spectrum and the mathematical expression are provided. Later, the scattered field is determined. Then, by boundary condition, a system of linear algebraic equations is obtained. Then, as the last step, the MAS method mentioned in the second subsection is employed. The solution answers the determination of the dielectric object's electrical size by electromagnetic scattering from the corresponding object.

A. *Brief explanation of the incident field*

In this section, the mathematical formulation and the geometry of the problem are provided. The study investigates the electrical properties of the material by a periodic pulse as an incident electromagnetic wave with the spectrum of the Hamming Window. Numerical analysis is done as the 2D problem. Therefore, the incident wave is considered as a line source with different and weighted frequency components as (1). In other words, for each frequency component in the incident wave, there is a weighting coefficient b_n as provided in (2). It should be highlighted that, throughout the study, time dependency is $e^{-i\omega t}$ (ω is the angular frequency).

$$E_z^{inc}(t,x,y) = \sum_{n=0}^{n=N} b(f_n) H_0^{(1)}\left(k_n\sqrt{(x-x_{inc})^2+(y-y_{inc})^2}\right) e^{-i2\pi f_n t} \tag{1}$$

Here, $b(f_n)$ stands for the spectrum of the incident signal, $H_0^{(1)}$is Hankel's function of the first kind and the zeroth order, the source location is at (x_{inc}, y_{inc}), $k_n = \frac{2\pi f_n}{c}, f_n = \frac{(f_h - f_l)n}{N} + f_l$, n is ranging from 0 to N, N+1 is the number of frequencies, and f_h and f_l correspond to the highest and lowest frequency in the predefined bandwidth. In our case f_l and f_h are equal to 38 and 52 GHz, respectively. As a result, we get a radio pulse that has the spectrum maximum amplitude at the 45 GHz frequency.

$$b(f_n) = 1 - \frac{0.46}{0.54}\cos\left(\frac{2\pi}{N}\cdot n\right), n = 0 \ldots N. \tag{2}$$

This form of Hamming window is not completely traditional, but it saves the amplitude of the peak in the time domain instead of saving the energy under the envelope. The key point in this approach is that the incident wave has a frequency band in which the weighting of each frequency component is determined by (2). Please note that, by changing N, one can change the period of the pulse.

After defining the incident wave, we consider the scattered field. To obtain uniquely the scattered field components, the boundary condition should be satisfied for all frequencies of the Hamming window. As a result, the scattered field at the desired

point, at the given frequency is found. For each frequency, the scattered field component is denoted as $E_z^{s,n}(f_n,x,y)$. Then, the envelope of the scattered signal in the time domain at the point (x,y,t) can be found as $\mathcal{E}_z^s(t,x,y)$.

$$\mathcal{E}_z^s(t,x,y) = abs\left[\sum_{n=0}^{N} E_z^{s,n}(f_n,x,y)e^{-i2\pi f_n t}\right] \tag{3}$$

Here, $t \in [0,T]$ and T is a period.

The echo of the object of interest should not be overlapped with the incidence wave and with itself. That's why we should take a period of the signal long enough by inspection. The length of the echo is larger than the incident signal because, inside the object, there are several reflections in the case of the dielectric. To describe electromagnetic scattering by the object, the propagating waves are considered. Therefore, the non-negative frequencies are analyzed in the frequency domain.

In the following section, the details on MAS and scattered field expression and how the boundary condition is satisfied are investigated. For each frequency, the analysis is done and their linear combination will provide the total field outcomes.

B. Direct problem solution using the MAS

Here, the main aim is to express the scattered field components in a mathematical form and satisfy the boundary conditions on the surface of each object for total fields. To solve the proposed problem, the MAS is employed [18], [22]. In conventional MAS, the sources representing the scattered field are shifted through the auxiliary surface and boundary conditions are still satisfied on the actual surfaces [18]. This approach eliminates the singularity problems in radiation integrals. In the regularized form of MAS, Hankel's function (Green's function in 2D problems) is regularized and singularity problems are solved by regularizing the kernel of the radiation integrals (Hankel's function) [19]. For smooth surfaces, MAS gives better results, whereas the regularized form of MAS is also suitable for discontinuous or complex surfaces.

For two-dimensional geometries, Green's function of Helmholtz's equation as given in (4) is Hankel's function.

$$\nabla^2 u + k^2 u = -\delta(x - x_{inc})\delta(y - y_{inc}) \tag{4}$$

Here u can be the z component of the electric or magnetic field. The solution of (4) will be $H_0^{(1)}(k\sqrt{(x-x_{inc})^2+(y-y_{inc})^2})$ with some constant. Then, if there exists a scatterer in the regions of interest, the scattered electric field can be expressed in terms of the convolution of Green's function of the governing equation and the induced current on the scatterer which models the scatterer in the free space as (5):

$$\mathrm{E}_z^s(\boldsymbol{\rho}) = \int_S J(\boldsymbol{\rho}')H_0^{(1)}(k|\boldsymbol{\rho}-\boldsymbol{\rho}'|)dl' \tag{5}$$

Here $J(\boldsymbol{\rho}')$ is the induced current on the scattering surface modeling the obstacle and S is the surface of the scatterer (Please refer to Fig. 1). Then, for MAS, the scattered field is approximated as [17, 23]:

$$\mathrm{E}_z^s(\boldsymbol{\rho}) \cong \sum_{i=1}^{N} J(\boldsymbol{\rho}_i'')H_0^{(1)}(k|\boldsymbol{\rho}-\boldsymbol{\rho}_i''|) \tag{6}$$

Please, notice that, $\boldsymbol{\rho}_i''$ is a vector that denotes discrete points on auxiliary surfaces as given in Fig. 1.

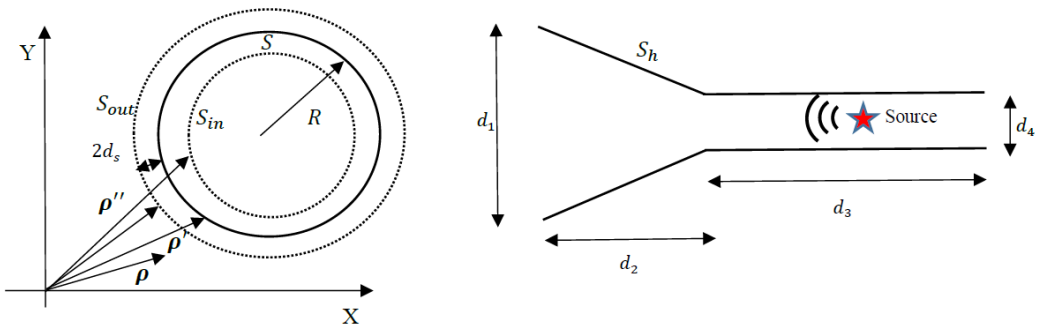

Fig. 1. Geometry of the problem, dielectric circular cylinder and the horn antenna.

In Fig. 1, the 2-D geometry of the scatterer surfaces (physical (solid line) and auxiliary (dashed lines) surfaces (contour in 2D case)), horn antenna, and position of the incident source are provided. As it is understood from the figure, there exists a dielectric two-dimensional scatterer in the space, and a line source is employed as the incident electric field $E_z^{inc}(x,y) = H_0^{(1)}(k\sqrt{(x-x_{inc})^2+(y-y_{inc})^2})$. The horn antenna is used to guide the incident electromagnetic field. The scattered field is also measured from the horn antenna. Such scenarios are investigated by MAS since the verification by experiment is aimed at similar scenarios.

The relative permittivity of the dielectric is given by ϵ_r, and outside is the vacuum. The sources on the outer auxiliary surface represent the field inside the object, whereas the inner ones stand for the field outside the object. It should be highlighted that the horn antenna surface is considered to be perfect electric conducting (PEC) and outside the dielectric object, the incident and scattered fields exist; however, inside the object, there is only a single field component. In Table 1, dimensions regarding the geometry of the problem are provided.

Table 1. The parameters and their dimensions

Parameter symbol	Parameter value (mm)	Parameter symbol	Parameter value (mm)
d_1	46	d_4	5.2
d_2	120	R	15 and 19
d_3	120	d_s	0.3 R

The electric field outside the object can be expressed as (7) [18, 19]:

$$E_{\text{out}}(x,y) = \sum_{n=1}^{N_d} X_n^{\text{in}} H_0^{(1)}\left(k_{\text{out}}\sqrt{(x-\text{x}_{in}^n)^2+(y-\text{y}_{in}^n)^2}\right) + \sum_{n=1}^{N_h} \text{Y}_n RH\left(k_{\text{out}}\sqrt{(x-\text{x}_h^n)^2+(y-\text{y}_h^n)^2}\right) + E_z^{inc}(x,y) \tag{7}$$

Here, $H_0^{(1)}$ is the Hankel functions of the first kind and zeroth order. RH is the regularized Hankel's function [19]. The first term at the right side of (4) represents the scattered field due to the dielectric object and X_n^{in} are the unknown complex-valued amplitudes of the auxiliary sources distributed on the inner auxiliary surface S_{in} at the points $(\text{x}_{in}^n, \text{y}_{in}^n)$. The second term at the right-hand side of (7) stands for the scattered field due to the horn antenna and Y_n-are the unknown complex-valued amplitudes of the auxiliary sources distributed on the horn and waveguide surface S_h, $(\text{x}_h^n, \text{y}_h^n)$ are the collocation points on the horn and waveguide's surface. Since the horn antenna surface is not smooth, regularized Hankel function is preferred as mentioned above.

In the same manner, the electric field inside the dielectric can be found as:

$$E_{\text{in}}(x,y) = \sum_{n=1}^{N} X_n^{\text{out}} H_0^{(1)}\left(k_{\text{in}}\sqrt{(x-\text{x}_{out}^n)^2+(y-\text{y}_{out}^n)^2}\right) \tag{8}$$

Again, X_n^{out} are the unknown complex-valued coefficients of the auxiliary sources spanned over the outer auxiliary contour S_{out} in points $(\text{x}_{out}^n, \text{y}_{out}^n)$. The magnetic field components inside and outside the scatterer can be expressed with the same approach. By Maxwell's equation (9), the magnetic field can be obtained:

$$\text{rot}\ \vec{E} = -i\omega\mu\vec{H} \tag{9}$$

where ω is the angular frequency, μ is permeability, and rot is the curl operator.

After that, to obtain the unknown complex amplitudes in field expression, the boundary conditions should be applied on the dielectric surface and horn antenna. For the dielectric interface, (10) should be satisfied on the surface whereas, the total tangential component of the electric field should be nullified on the PEC surface (horn antenna) as (11).

$$E_{\text{in}}(\text{x}_d^n, \text{y}_d^n) = E_{\text{out}}(\text{x}_d^n, \text{y}_d^n),$$

$$H_{\text{in}}\left(\mathrm{x}_d^n, \mathrm{y}_d^n\right) = H_{\text{out}}\left(\mathrm{x}_d^n, \mathrm{y}_d^n\right) \tag{10}$$

$$E_{\text{in}}\left(\mathrm{x}_h^n, \mathrm{y}_h^n\right) = 0 \tag{11}$$

In other words, the tangential components of the total electric and magnetic field are continuous on dielectric surface $S\left(\mathrm{x}_d^n, \mathrm{y}_d^n\right)$ whereas, the total tangential electric field should be zero on the horn antenna surface $S_h(\mathrm{x}_h^n, \mathrm{y}_h^n)$. After satisfying the boundary conditions for specified observation points, a system of linear algebraic equations is attained, and then, by inversion, the unknown complex-valued coefficients of unknowns X_n^{in}, X_n^{out}, and Y_n are found. Keep in mind that the time complexity of the matrix inversion in MatLab is $O(n^3)$. This gives the ability to find the field distribution inside and outside the dielectric scatterer.

3. Experimental setup details

Real measurement was carried out for two samples of Plexiglas dielectric cylinders of 180 and 148 mm in height and 38 and 30 mm in diameter, respectively, which are marked as objects 1 and 2. Time-domain signals were obtained by synthesizing from measurement data of the scalar reflection coefficient on the frequency grid in the range of 38-52 GHz. Synthesis of time-domain signals was carried out using the discrete Fourier transform. In the frequency domain, a Hamming weight window was applied to eliminate spurious side lobes in the time domain. Information about the phase of the useful signal under interest was stored due to the use of the Fourier-holography principle in frequency-time space [24], where the source of the reference signal is the reflection from the junction of the waveguide and the horn. A horn with a length of 120 mm and aperture size of 46×46 mm as a probe and a waveguide with a cross-section of 5.2×2.6 mm was used. Such a horn design ensures that the useful reference reflection dominates over the reflection from the aperture, which introduces interfering components. This fact simplifies the interpretation of the synthesized signal in the time domain.

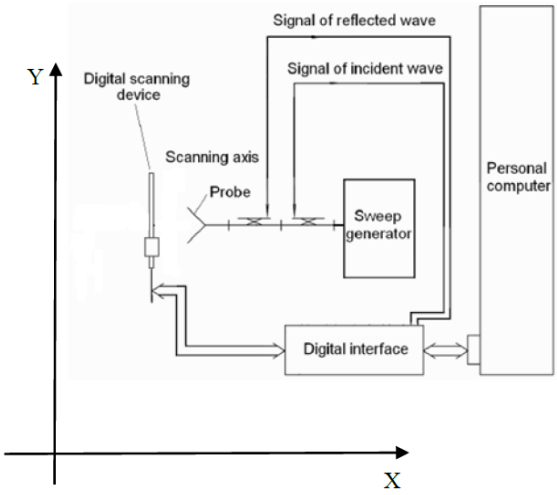

Fig. 2. Experimental setup

The experimental setup [12] consists of a sweep generator, the output signal of which propagates through a scalar reflectometer, which consists of two directional couplers. The first directional coupler with an appropriate detector allows us to get information about the power of the signal that is fed to the radiator. To receive the reflected signal, the same horn is used for radiation. The second directional coupler with a detector is designed to measure the power of the signal that returned to the waveguide after reflection from the object under study. Both detectors are assumed to operate in quadratic mode. The ratio of the power of the reflected signal to the power of the radiated signal makes it possible to estimate the value of the inserted reflection coefficient in the presence of a reference reflection. The signals measured by the detectors are converted into digital form in the digital interface and transferred to a personal computer. The movement of the object under study in the direction perpendicular to the radiation axis is performed using a stepper motor, which is controlled via a digital interface from a personal computer. Thus, scanning of the object is provided not by moving the probe past the object, but by moving the object past the probe.

The measurement procedure involves placing the object at the desired point in space, carrying out measurements in the frequency band on a discrete grid, repeating the measurements the number of times specified by the program, applying median averaging, data transformation from the frequency domain to the time domain, moving the object to the next spatial position, repeating the measurements. Instead of the discrete Fourier transform, methods of parametric spectral analysis can be applied, in

particular, Prony's method [25], and the maximum likelihood method [13] with increasing the order of the model, they have a higher level of resolution.

4. Results of the numerical experiments and comparison with the real experiment

Based on the above-described mathematical model the computer program was created in MATLAB and the numerical results are obtained. The calculations are done on the processor Intel(R) Core(TM) i7-8700K, CPU (3.70 GHz), and installed RAM 32.0 GB. For each figure, results are obtained approximately in 20 seconds. The case when the circular dielectric cylinder has the permittivity $\varepsilon = 2.56 + 0.04i$ is considered. The object is irradiated by the horn antenna. The Incident field propagates along the *x*-axis in the negative direction. As it was mentioned in the theoretical part, the incident field is a periodic pulse with the spectrum of the Hamming window. The source of this pulse is located in the middle of the waveguide. The scattered field is measured near the horn-waveguide connection at 1cm from the horn inside the waveguide. The period of the pulse repetition is T=3.57 ns.

Figure 3 shows the comparison of the numerical and experimental results. Object 1 is at a distance of 390 mm from the junction of the waveguide and the horn or 270 mm from the horn aperture plane. Dependences of the reflectivity $\left(|\Gamma| = \frac{|\mathcal{E}_z^s(t,x,y)|}{|E_z^{inc}(t,x,y)+\mathcal{E}_z^s(t,x,y)|}\right)$ on the X and Y axis are given. On the left figure, we see two peaks. The first peak corresponds to the reflection by the front part of object 1 and the second peak corresponds to the reflection from the rear part of object 1. The wave covers the distance from the front part to the rear part two times and the permittivity of the object determines the speed of the wave which is inversely proportional to the square root of the permittivity. So, the distance between the first and the second peak gives the ability to determine the electric size of the dielectric object. The right figure corresponds to the reflections from the front and back parts of the cylinder in the Y section. The right figure is like the image of the object. For the first case, the radius of the object *R* is taken as 15 mm. If we initially know the permittivity of the object, we can find its radius with a precision of 1%. We see very good agreement between the simulation outcomes and the experiment results. The extra peaks in the experimental graph are caused by interaction with the measurement equipment. An experiment was conducted not in the Anechoic chamber that's why there are reflections also from the objects around.

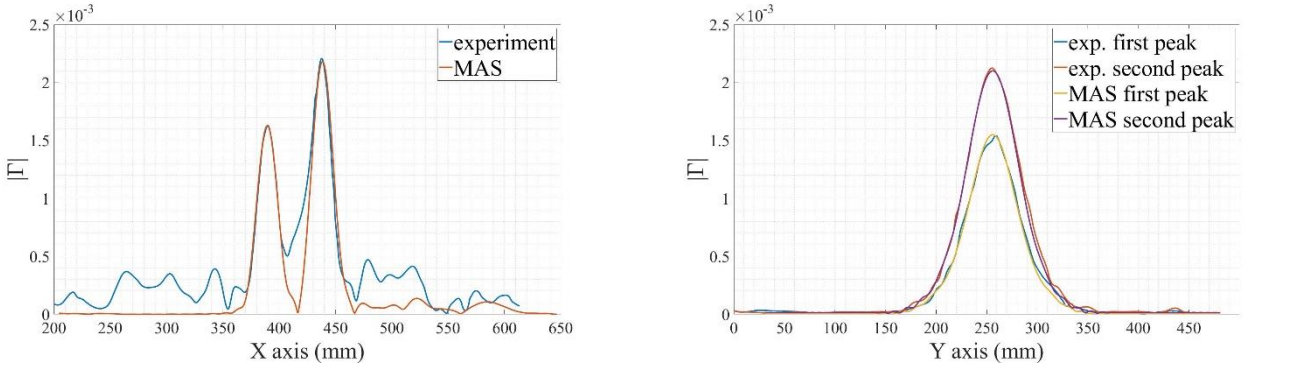

Fig. 3. The scattered signal at the waveguide along X and Y axes at a distance between the object and the junction of the waveguide d=390 mm, experimental and simulation results, *R*=15 mm.

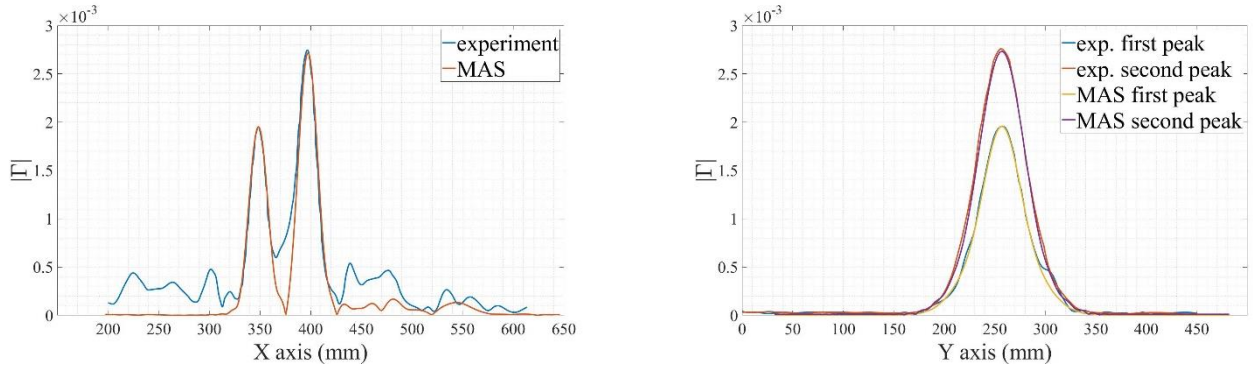

Fig. 4. Scattered signal at the waveguide along X and Y axes at a distance between the object and the junction of the waveguide d=350 mm, experimental and simulation results, *R*=15 mm.

Figure 4 stands for the comparison of the numerical and experimental results. The object is at a distance of 350 mm from the junction of the waveguide and the horn or 230 mm from the horn aperture plane. Dependences of the reflectivity (|Γ|) on the x and y axis are obtained. The radius of the object is *R*=15mm. Here also we can find the object radius with a precision of 1%.

Figure 5 reveals the comparison of the numerical and experimental results. The object is at a distance of 300 mm from the junction of the waveguide and the horn or 180 mm from the horn aperture plane. Dependences of the Reflectivity on the X and Y axis are provided. The radius of the object is R=15mm. Here we can find the object radius with a precision of 2%.

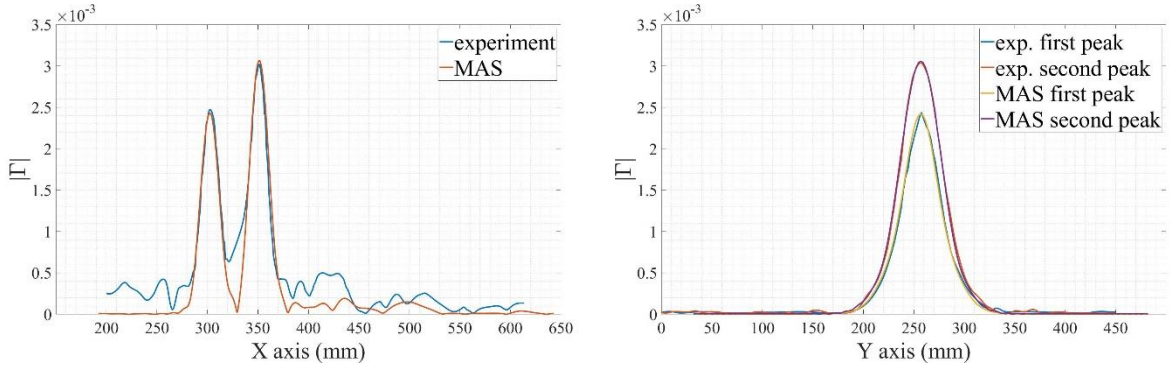

Fig. 5. The scattered signal at the waveguide along X and Y axes at a distance between the object and the junction of the waveguide d=300 mm, experimental and simulation results, *R*=15 mm.

Figure 6 again shows the comparison of the numerical and experimental results. Object 2 is at a distance of 450 mm from the junction of the waveguide and the horn or 330 mm from the horn aperture plane. Dependences of the Reflectivity on the X and Y axis are given. The radius of the object is R=19 mm. Here we can find the object radius with a precision of 3%.

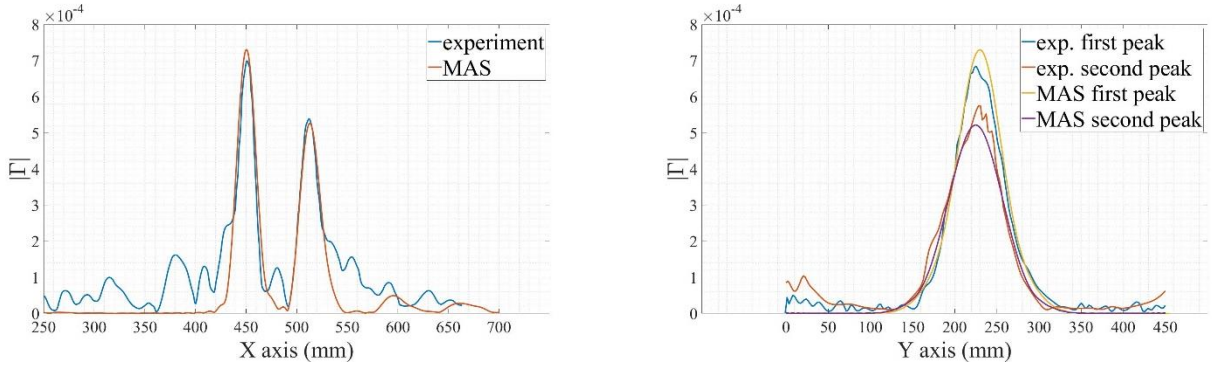

Fig. 6. The scattered signal at the waveguide along X and Y axes at a distance between the object and the junction of the waveguide *d*=450 mm, experimental and simulation results, *R*=19 mm.

5. Conclusion

In this article, there was considered the diffraction problem of the periodic EM pulse irradiated by the horn antenna, by the dielectric circular cylinder. The method of auxiliary sources was used for the solution of the stated problem. The dielectric circular cylinders of 2 different radii were considered and their electric size was determined by the analysis of the pulse echo. The simulation results are compared to the experimental ones and good agreement between the simulation and experimental results is shown. In the future, we plan to consider the case when the object is behind the dielectric slab. The correctness of the determination of the electric size of the object by the analysis of the scattered pulse echo serves as the verification of the approach. The outcomes reveal that less than a 3% deviation is observed between numerical and experimental analysis. Since we reached a good agreement with the experimental and numerical analysis. In the future, the proposed approach can be used to obtain the scattering data for different scenarios to train a neural network that can be employed in unknown object recognition by electromagnetic waves.

6. References

[1] M. T. Bevacqua, G. G. Bellizzi, T. Isernia, and L. Crocco, "A Method for Effective Permittivity and Conductivity Mapping of Biological Scenarios via Segmented Contrast Source Inversion," *Prog. Electromagn. Res.*, vol. 164, no. November 2018, pp. 1–15, 2019.

[2] B. Saçlı *et al.*, "Microwave dielectric property based classification of renal calculi: Application of a kNN algorithm," *Comput. Biol. Med.*, vol. 112, p. 103366, 2019.

[3] E. Sever, Y. A. Tuchkin, and F. Dikmen, "On a superalgebraically converging, numerically stable solving strategy for electromagnetic scattering by impedance cylinders," *J. Comput. Electron.*, vol. 17, no. 1, pp. 427–435, 2018.

[4] C. E. Athanasiadis, E. S. Athanasiadou, and P. Roupa, "On the Far Field Patterns for Electromagnetic Scattering in Two Dimensions," *Reports Math. Phys.*, vol. 89, no. 2, pp. 253–265, 2022.

[5] E. Sever, F. Dikmen, and Y. A. Tuchkin, "Superalgebraically converging Galerkin method for electromagnetic scattering by dielectric cylinders," *Radio Sci.*, vol. 52, no. 10, pp. 1282–1292, 2017.

[6] H. Onal, T. Yilmaz, and M. N. Akinci, "A BIM-Based Algorithm for Quantitative Monitoring of Temperature Distribution during Breast Hyperthermia Treatments," *IEEE Access*, 2023.

[7] X. Chen, Z. Wei, M. Li, and P. Rocca, "A Review of Deep Learning Approaches for Inverse Scattering Problems," *Prog. Electromagn. Res.*, vol. 167, no. June, pp. 67–81, 2020.

[8] O. A. Pryshchenko *et al.*, "Implementation of an Artificial Intelligence Approach to GPR Systems for Landmine Detection," *Remote Sens.*, vol. 14, no. 17, p. 4421, 2022.

[9] O. O. Drobakhin, V. V Alekseev, and A. I. Chekh, "Microwave multifrequency radar images of dielectric structures," in *2008 4th International Conference on Ultrawideband and Ultrashort Impulse Signals*, 2008, pp. 256–258.

[10] G. Borgioli *et al.*, "A hologram reconstruction algorithm for landmine recognition and classification based on microwave holographic radar data," in *2018 Progress in Electromagnetics Research Symposium (PIERS-Toyama)*, 2018, pp. 1938–1944.

[11] I. Ivanchenko, M. Khruslov, N. Popenko, V. Plakhtii, D. Rönnow, and Y. Shestopalov, "A novel resonance method for determining the complex permittivity of local inclusions in a rectangular waveguide," *Meas. Sci. Technol.*, vol. 31, no. 9, p. 97001, 2020.

[12] O. O. Drobakhin, V. V Alekseev, M. V Andreev, Y. V Kondratyev, and D. Y. Saltykov, "Multifrequency near-zone radar of 6-mm wave range with combination of pulse synthesis and transversal scanning," *Telecommun. Radio Eng.*, vol. 66, no. 10, 2007.

[13] M. V Andreev, V. F. Borul'ko, and O. O. Drobakhin, "Resolvability of spectrum analysis with the help of the method of maximum likelihood," *Radioelectron. Commun. Syst*, vol. 41, no. 1, pp. 3–11, 1998.

[14] O. O. Drobakhin and V. G. Korotkaya, "Use Of Prony Method For Measuring The Thickness Of Layered Dielectrics," *Sov. J. Nondestruct. TESTING-USSR*, vol. 23, no. 5, pp. 315–323, 1987.

[15] V. Tabatadze, D. Kakulia, G. Saparishvili, R. Zaridze, and N. Uzunoglou, "Development of a new efficient numerical approach for buried object recognition," *Sens. Imaging*, vol. 12, no. 1–2, pp. 35–56, 2011, doi: 10.1007/s11220-011-0060-7.

[16] V. D. Kupradze, "On the approximate solution of problems in mathematical physics," *Russ. Math. Surv.*, vol. 22, no. 2, p. 58, 1967.

[17] R. Zaridze, G. Bit-Babik, K. Tavzarashvili, N. K. Uzunoglu, and D. Economou, "The method of auxiliary sources (MAS)—Solution of propagation, diffraction and inverse problems using MAS," in *Applied Computational Electromagnetics*, Springer, 2000, pp. 33–45.

[18] V. Tabatadze, K. Karaçuha, and E. Karaçuha, "Body Shape and Complex Permittivity Determination Using the Method of Auxiliary Sources," *Prog. Electromagn. Res.*, vol. 87, pp. 115–125, 2019.

[19] V. Tabatadze, K. Karaçuha, Ö. F. Alperen, and R. Zaridze, "A New Numerical Approach To Electromagnetic Eigenvalue Problem And Wave Scattering By Conducting Complex-Shaped Geometries: Gaussian Basis And Regularized Hankel Functions," *J. Appl. Electromagn.*, vol. 24, no. 1, 2022.

[20] H. T. Anastassiu, D. G. Lymperopoulos, and D. I. Kaklamani, "Accuracy analysis and optimization of the method of auxiliary sources (MAS) for scattering by a circular cylinder," *IEEE Trans. Antennas Propag.*, vol. 52, no. 6, pp. 1541–1547, 2004.

[21] H. T. Anastassiu, D. I. Kaklamani, D. P. Economou, and O. Breinbjerg, "Electromagnetic scattering analysis of coated conductors with edges using the method of auxiliary sources (MAS) in conjunction with the standard impedance boundary condition (SIBC)," *IEEE Trans. Antennas Propag.*, vol. 50, no. 1, pp. 59–66, 2002.

[22] V. Tabatadze, K. Karaçuha, and R. Zaridze, "Electromagnetic Scattering from 2-D Conducting Objects with Arbitrary Smooth Shape: Complete Mathematical Formulation of the Method of Auxiliary Sources for E-Polarized Case."

[23] R. Zaridze, G. Bit-Babik, K. Tavzarashvili, D. P. Economou, and N. K. Uzunoglu, "Wave field singularity aspects in large-size scatterers and inverse problems," *IEEE Trans. Antennas Propag.*, vol. 50, no. 1, pp. 50–58, 2002, doi: 10.1109/8.992561.

[24] O. O. Drobakhin and V. A. Karlov, “Holographic approach to microwave measurement,” in *Proc. of the 16th URSI Int. Symp. on Electromagnetic*, 1998, vol. 1, pp. 109–111.
[25] M. V Andreev and O. O. Drobakhin, “Feature of Prony’s method application for natural frequencies estimation from the frequency response,” in *2016 8th International Conference on Ultrawideband and Ultrashort Impulse Signals (UWBUSIS)*, 2016, pp. 18–20.

Received 7 February 2023